End-Capped Associative Polymer Chains between Nanospheres: Attractions in Ideal Solutions

Surita R. Bhatia[†] and William B. Russel*

Department of Chemical Engineering, Princeton University, Princeton, New Jersey 08544

Received January 18, 2000; Revised Manuscript Received May 15, 2000

ABSTRACT: We calculate equilibrium configurations of telechelic associative polymer chains without excluded volume interactions between flat plates and curved surfaces, obtaining analytical expressions for flat plates and numerical results for chains between two spheres. Ideal chains with strongly but reversibly adsorbed terminal groups produce an attraction of $O(kT)$ per chain for planar surfaces as opposed to $\ll kT$ per chain in marginal and good solvents at high densities. Our numerical results for two spheres yield a weaker repulsion and an attraction of shorter range than predicted by the Derjaguin approximation based on the flat plate solution. These effects are due to deflection of chains out of the gap at close separations.

Introduction

The interaction between adsorbing polymer chains and solid surfaces has been the subject of much study, both theoretical and experimental. Good models for the polymer layer are crucial to the understanding of sterically stabilized colloidal particles and are useful in describing block copolymer micelles, star polymers, and block copolymer microphases. The simplest model for chains grafted to a flat surface at one end is the Alexander−de Gennes treatment for polymer brushes,[1] a scaling theory that assumes a steplike segment density profile with all chain ends residing at the edge of the brush. While producing the correct functional dependence for the brush height, this picture obviously gives no insight into details of the brush structure. The self-consistent field (SCF) approach of Milner, Witten, and Cates represents a considerable improvement, yielding a parabolic segment density profile for strongly stretched chains in a good solvent.[2] Self-consistent lattice models,[3,4] Monte Carlo simulations,[5,6] scaling theories,[7] and molecular dynamics (MD) calculations have examined the effects of graft density, solvent quality, chain branching, and molecular weight in more detail.

Extending these results to curved surfaces is not trivial. For surfaces with low curvature, the Derjaguin approximation[8] perturbs results from flat plates, but surfaces with moderate to high curvatures present some difficulties. Daoud and Cotton[9] modified the Alexander−de Gennes model for spherical surfaces by allowing the blob size to increase with distance from the core, but still assumed all chain ends to reside at the brush edge. Dan and Tirrell[10] applied the Dolan−Edwards SCF method[11] to examine the effects of surface curvature on end-grafted polymer chains, finding significant deviations from planar interfaces at curvatures of the same order as the chain dimensions. This approach and the lattice counterpart[12] couple excluded volume in the mean field approximation to the local segment density. Their results for the segment density profiles agree well with results from MD simulations, but only with scaling theory in the limit of high surface curvature or large molecular weight. Li and Witten[13] developed a variational approach for polymer brushes attached to spherical and cylindrical surfaces in the strong stretching limit, finding good agreement between their results and asymptotic solutions for flat plates and cylinders. Wijmans and Zhulina[14] implemented Scheutjens−Fleer lattice calculations to compute segment density profiles for polymer brushes grafted to spheres. Although similar in spirit to the Dolan−Edwards SCF theory used by Dan and Tirrell, this approach does not linearize the dependence of the free energy on the local segment density. Wijmans and co-workers[15] later extended the computations to pair potentials between spheres by adopting a two-dimensional lattice in a cylindrical coordinate system and allowing the segment density to vary in both the axial (line-of-centers) and radial directions. They found the repulsion for curved surfaces to be softer than predicted by the Derjaguin approximation, primarily because of the movement of chains out of the gap between the surfaces.

More recently, there has been increased interest in associative polymers, which contain more than one group that can absorb to a surface. In practice, these are typically hydrophobically modified water-soluble polymers, triblock copolymers, or ionomers. Milner and Witten[16] adapted SCF calculations to telechelic polymers, with an absorbing group at each end of the chain, between flat plates. The absorption was assumed to be strong enough to ensure that a chain starting on one surface will either form a loop back to that surface or bridge to the other. For strongly stretched chains with a parabolic segment density profile extending to a distance L, Milner and Witten find an attractive minimum in the free energy near a separation of $2L$, or close to brush contact, due to the increased entropy of $O(kT)$ per bridge in the contact zone.[16] Numerical results for chains in a marginal solvent are presented and extended by scaling arguments to good solvents and melts. Santore et al.[17] addressed associative polymers between flat plates, without constraining the absorbing groups to lie on the surface and allowing for depletion of chains in the gap. When absorption is sufficiently strong, the calculations yielded a bridging attraction of about 0.2 kT per chain, which decreases as the solvent quality

[†] Present address: Department of Chemical Engineering, University of Massachusetts Amherst, 686 N. Pleasant St., Amherst, MA 01003-3110.

10.1021/ma0000677 CCC: $19.00
Published on Web 07/06/2000

increases. Similar results are obtained by Björling[18] and Björling and Stilbs,[19] who examined the good solvent case for flat plates numerically using a Scheutjens−Fleer approach. For the "symmetrical case" in which both surfaces are covered with polymers, they find a weaker attraction than Milner and Witten did for the marginal solvent case. Again, the corresponding problem with curved surfaces is considerably more difficult. Semenov and co-workers[20] extended the results of Milner and Witten[16] and Johner and Joanny[21] to polymeric micelles for micellar cores small relative to the overall micelle size via scaling arguments, assuming an attraction of kT per chain in the contact area. However, to our knowledge no analytical or numerical results have been published on associative polymers between surfaces with a finite curvature.

In this analysis, we use the Dolan−Edwards[11] approach to treat telechelic associative polymers, neglecting both excluded and physical volume (i.e., ideal chains). This simplification allows us to examine easily a range of molecular weights, which can be difficult with either the full SCF or MD simulations because of the computing time necessary. It is also useful for examining chain dimensions that are on the order of the surface curvature. Simple analytical expressions can be extracted for some geometries, which can be useful in comparing experimental results to theory.

We begin by applying the results for end-grafted polymers on flat plates to telechelic polymers and demonstrate that an attractive minimum is still obtained for ideal chains. We then solve for the segment density and free energy of polymers attached at both ends to an isolated sphere. Finally, we solve the equations in bispherical coordinates numerically for chains between two spheres and compare this to predictions based on the Derjaguin approximation.

Diffusion Equation Model

In this model, we consider the density of configurations available to a subchain of s segments, beginning at $\mathbf{r}'$ and ending at $\mathbf{r}$, denoted $G(\mathbf{r}, \mathbf{r}', s)$. The total number of segments in the chain is denoted N, and l is the segment length. For an ideal chain, the differential equation for G reduces to[11]

$$\frac{\partial G}{\partial s} = \frac{l^2}{6}\nabla^2 G \tag{1}$$

The segment density at any position $\mathbf{r}$ is related to the probability that a subchain of length s will meet a subchain of length $N - s$ at $\mathbf{r}$. This must be integrated over all end points and segment positions along the chain:

$$n(r) \propto \int_V \int_V \int_0^N G(\mathbf{r}, \mathbf{r}', s) G(\mathbf{r}'', \mathbf{r}, N - s) \mathrm{d}\mathbf{r}' \, \mathrm{d}\mathbf{r}'' \mathrm{d}s \tag{2}$$

The partition function for a chain is obtained by summing up the total number of configurations

$$W = \int_V \int_V G(\mathbf{r}'', \mathbf{r}', N) \, \mathrm{d}\mathbf{r}' \, \mathrm{d}\mathbf{r}'' \tag{3}$$

and determines the Helmholtz free energy per chain as

$$\frac{A}{kT} = \ln \frac{n}{N} - 1 - \ln W \tag{4}$$

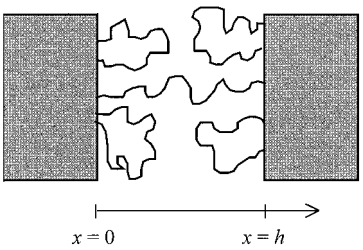

Figure 1. Arrangement of associative triblocks between two flat plates.

Since we only consider ideal chains in this work, it is not necessary to account for the surface density of chains as an additional parameter. The chains do not interact and hence do not feel any difference as the surface density of chains is increased. The layer thickness for such chains is independent of surface coverage, and the free energy of the layer is proportional to the free energy of a single chain. Thus, it is sufficient to solve eqs 1−4 for a single chain, multiplying by the total number of chains when appropriate.

Results for Flat Plates

Dolan and Edwards[11] derived solutions for terminally anchored chains on flat plates, which we use to investigate the behavior of end-capped associative polymers between flat plates as depicted in Figure 1. In doing so, we assume that the association is strong enough that the chain ends always reside on a surface. The appropriate differential equation and boundary conditions are

$$\frac{\partial G}{\partial s} = \frac{l^2}{6}\frac{\partial^2 G}{\partial x^2} \tag{5}$$

$$G(0, x', s) = 0 \tag{6a}$$

$$G(h, x', s) = 0 \tag{6b}$$

$$G(x, x', 0) = \delta(x - x') \tag{6c}$$

The first two boundary conditions, eq 6 parts a and b, prevent the chain from penetrating the flat plates. The final boundary condition, eq 6c, requires the chain to start at x'. If we choose $x' = 0$, the only solution to eqs 5 and 6 will be $G = 0$. Instead, Dolan and Edwards start the chain a small distance, on the order of the segment length l, off the surface.[11] They argue that because the first segment of the chain is fixed at the surface, the random walk of the chain effectively begins at the second segment.

We can also derive boundary conditions by applying the relationship between the probability density for a segment and the preceding segment at the surface and recognizing that $\partial G/\partial s$ is $O(1/N)$, leading to[22]

$$\frac{1}{2}\frac{\partial G}{\partial x} - G = 0 \tag{7}$$

at $x = 0$ and h. Since this resembles a Taylor series expansion for G about $-l/2$, we set $G = 0$ on the surface and take the point of attachment to be half a segment length off the surface. These boundary conditions are equivalent to eq 6, with $x' = l/2$ or $x' = h - l/2$.

Scaling distance, position, and the probability density as $\bar{x} = x/N^{1/2}l$, $\bar{s} = s/N$, and $\bar{G} = N^{1/2}lG$, we obtain

$$\frac{\partial \bar{G}}{\partial \bar{s}} = \frac{1}{6}\frac{\partial^2 \bar{G}}{\partial \bar{x}^2} \tag{8}$$

$$\bar{G}(0, \bar{x}, \bar{s}) = 0 \tag{9a}$$

$$\bar{G}(\bar{h}, \bar{x}, \bar{s}) = 0 \tag{9b}$$

$$\bar{G}(\bar{x}, \bar{x}', 0) = \delta(\bar{x} - \bar{x}') \tag{9c}$$

where $\bar{h} = h/N^{1/2}l$ and $\bar{x}' = x'/N^{1/2}l = {}^1/_2N^{-1/2}$. Thus, we would expect that $\bar{G}(\bar{x}, \bar{x}, \bar{s})$ depends on $\bar{h}$ and N as well.

For plates at an infinite separation, the solution to eqs 5 and 6 near either plate is[22]

$$G(x, x', s) = \left(\frac{3}{2\pi s l^2}\right)^{1/2}\left[\exp\left(-\frac{3(x-x')^2}{2sl^2}\right) - \exp\left(-\frac{3(x+x')^2}{2sl^2}\right)\right] \tag{10}$$

To obtain the number of configurations for a chain with one end attached to the surface, we set $x' = l/2$ and integrated over all x to determine the free energy per chain as

$$\frac{A}{kT} = -\ln\left[\int_0^\infty G(x, x', N)\,dx\right] = -\ln\left[\operatorname{erf}\sqrt{\frac{3}{8N}}\right] \approx \frac{1}{2}\ln\left[\frac{2\pi N}{3}\right] + O\left(\frac{1}{N}\right) \tag{11}$$

for large N. For chains with both ends attached to the surface, we set $x' = l/2$ and require the other end of the chain to lie within $0 \le x \le l$. This is approximately the density of configurations for the entire chain evaluated at $x = l/2$, multiplied by l:

$$\frac{A}{kT} = -\ln\left[\int_0^l G(x, x', N)\,dx\right] \approx -\ln[lG(l/2, l/2, N)] \approx \frac{1}{2}\ln\left[\frac{2\pi N}{3}\right] + \ln\left[\frac{2N}{3}\right] - O\left(\frac{1}{N}\right) \tag{12}$$

So, the free energy is increased by the additional constraint.

For finite values of h, the solution to eqs 5 and 6 is an eigenfunction expansion:[11]

$$G(x, x', s) = \sum_{m=1}^{\infty}\frac{2}{h}\sin\left[\frac{m\pi x}{h}\right]\sin\left[\frac{m\pi x'}{h}\right]\exp\left[-\frac{m^2\pi^2 l^2 s}{6h^2}\right] \tag{13}$$

To apply this solution to the single-chain problem for many chains in the gap, we normalize the segment density on the total number of segments. For the case of telechelic associative polymers, the segment density will have contributions from both loops and bridging chains, i.e., chains starting on the left wall and ending on the left wall

$$n_1(x) \propto l\int_0^N G\left(x, \frac{l}{2}, s\right)G\left(x, \frac{l}{2}, N - s\right)ds \tag{14a}$$

chains starting on the left wall and ending on the right wall

$$n_2(x) \propto l\int_0^N G\left(x, \frac{l}{2}, s\right)G\left(x, h - \frac{l}{2}, N - s\right)ds \tag{14b}$$

and chains starting on the right wall and ending on the right wall

$$n_3(x) \propto l\int_0^N G\left(x, h - \frac{l}{2}, s\right)G\left(x, h - \frac{l}{2}, N - s\right)ds \tag{14c}$$

The probability density is then normalized such that

$$\int_0^h \{n_1(x) + n_2(x) + n_3(x)\}\,dx = 2Nn_p \tag{15}$$

where n_p is the surface density of chains on one plate.

We can use eqs 13 and 14 to determine the segment density profiles for a range of separations as shown in Figure 2, where 50 terms of the series in eq 13 were used to calculate G. The dashed and solid lines indicate contributions from bridging and looped chains, respectively. As expected, more bridges form as the plates move closer together. Figure 3 shows the fraction of segments belonging to bridging chains, f_{bridge}, at various separations. Bridging becomes significant when the surfaces are closer than $2N^{1/2}l$, with $f_{\text{bridge}} \approx 0.1$ at $h/N^{1/2}l = 1.75$. The fraction of bridges eventually levels off at ${}^1/_3$ for small separations. Physically, this means that the three options available to a chain (i.e., a loop on the left side, a loop on the right side, or a bridge) are equally favorable at close separations.

The free energy per chain, relative to the free energy of an isolated plate with loops of associative polymers, given by

$$\frac{\Delta A}{kT}(h) = -\ln\left[\frac{G\left(\frac{l}{2}, \frac{l}{2}, N\right)_h + G\left(\frac{l}{2}, h - \frac{l}{2}, N\right)_h}{G\left(\frac{l}{2}, \frac{l}{2}, N\right)_{h\to\infty}}\right] \tag{16}$$

is shown in Figure 4. The minimum at $h/N^{1/2}l \approx 1.0$ due to the bridging chains corresponds to an attraction between the plates. This attractive minimum, which is independent of N, is about 0.6 kT per chain.

It is interesting to compare this value with the attractive minima obtained by Milner and Witten[16] and Björling[18] and Björling and Stilbs[19] for marginal and good solvents, respectively. For marginal solvents, Milner and Witten have shown through both scaling arguments and numerical self-consistent field calculations that the minimum in the free energy scales as[16]

$$\frac{\Delta A_{\min}}{kT} = \left(\frac{R_o}{L}\right)^2 \sim \left[\frac{N^{1/2}l}{Nl(\sigma v/l)^{1/3}}\right]^2 \sim \frac{l^{2/3}}{N\sigma^{2/3}v^{2/3}} \tag{17}$$

where R_o is the end-to-end distance of the relaxed chain, L is the brush height, σ is the graft density, and v is the excluded volume parameter. For moderately long chains, the attraction per chain is rather weak and less than the value we obtain for ideal chains. As v increases and excluded volume effects become more important, the minimum grows weaker. The attraction, which occurs when the layers just overlap, is dominated by interpenetration near the brush edge.[16] The relevant length scale is then ξ_o, the fluctuation correction to the brush height or "roughness" of the brush.[19,20] Using a Scheutjens−Fleer approach, Björling and Stilbs[19] were able to show that the free energy for an athermal solvent with $v/l^3 = 1$ scales as $1/(\sigma\xi_o^2)$; alternatively, this can be expressed in terms of the brush height, leading to the same dependence of $\Delta A_{\min}$ on the graft density and molecular weight:

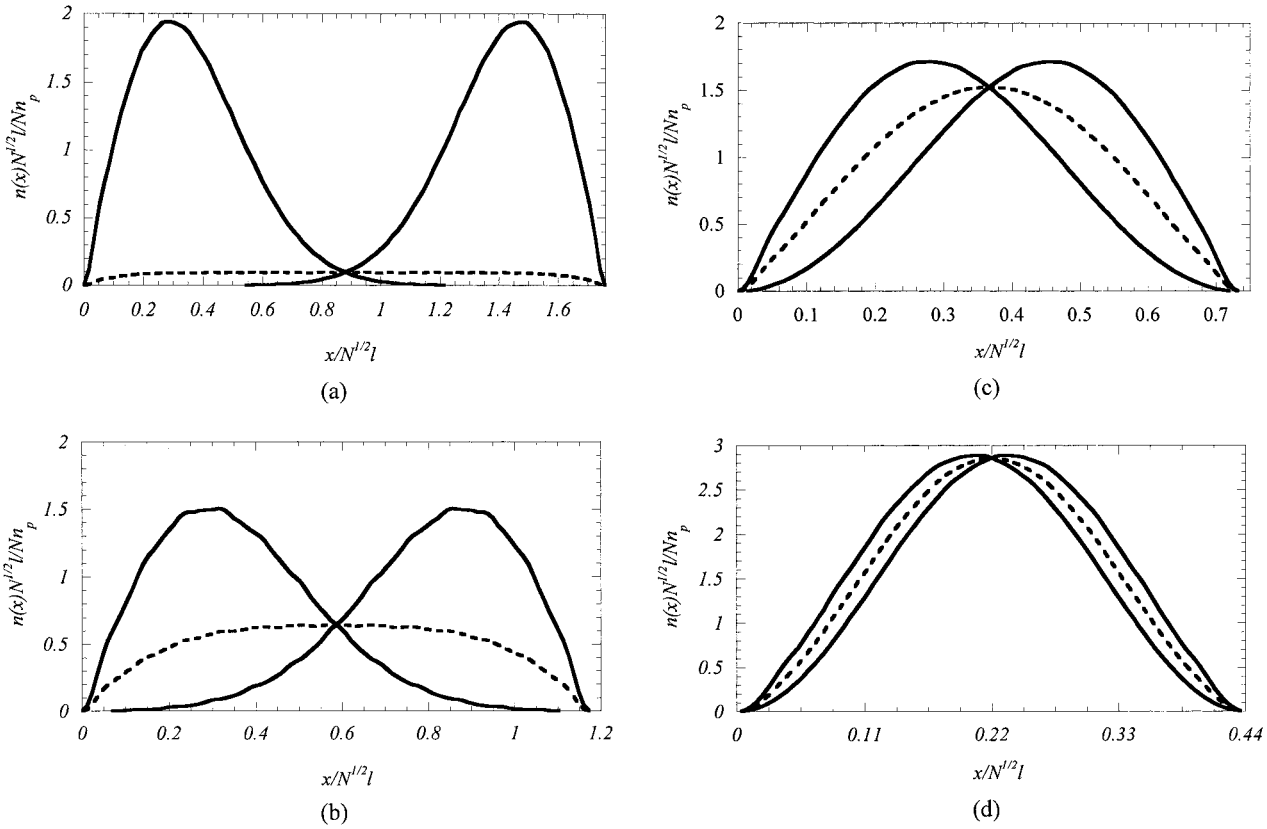

Figure 2. Segment density profiles between two flat plates. Dashed lines indicate segments belonging to bridges; solid lines indicate segments belonging to loops. (a) $h/N^{1/2} = 1.76$; (b) $h/N^{1/2} = 1.17$; (c) $h/N^{1/2} = 0.73$; (d) $h/N^{1/2} = 0.44$.

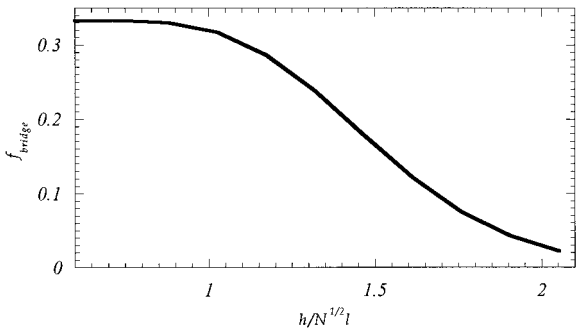

Figure 3. Fraction of segments belonging to bridging chains for telechelic polymers between flat plates.

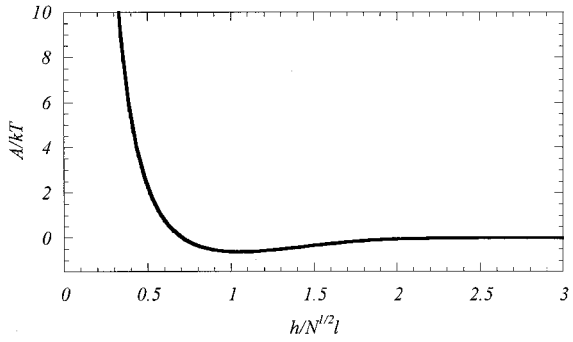

Figure 4. Free energy per chain for telechelic chains between flat plates as a function of normalized separation.

$$\frac{\Delta A_{\min}}{kT} \approx \left\{ \begin{matrix} \dfrac{0.4}{\sigma \xi_o^{\,2}} \\ 0.4\left(\dfrac{R_o}{L}\right)^2 \end{matrix} \right\} \sim \frac{0.4}{N^{0.784} l^{4/3} \sigma^{2/3}} \qquad (18)$$

where the Flory exponent is set to 0.588. Our result follows a similar scaling; since $R_o/L = O(1)$ for ideal chains, we again have $\Delta A_{\min}/kT \sim (R_o/L)^2 = 0.6$, which is stronger than either the marginal or good solvent results. Figure 5 shows the minima for the ideal, marginal, and good solvent regimes, demonstrating that excluded volume effects moderate the attractive forces between surfaces. Thus, our result for ideal chains should provide an upper limit on the strength of this bridging attraction.

Chains Anchored to Spherical Surfaces

For chains attached to a sphere (Figure 6), the geometry is still one-dimensional and the differential equation for G can be solved analytically:

$$\frac{\partial G}{\partial s} = \frac{l^2}{6}\frac{1}{r^2}\frac{\partial}{\partial r} r^2 \frac{\partial G}{\partial r} \qquad (19)$$

with the boundary conditions

$$G(a, r_o, s) = 0 \qquad (20a)$$

$$G(\infty, r_o, s) = 0 \qquad (20b)$$

$$G(r, r_o, 0) = \frac{1}{4\pi a^2}\delta(r - r_o) \qquad (20c)$$

where a is the radius of the sphere and $r_o = a + l/2$ is the point of attachment. The factor of $4\pi a^2$ in the initial condition reflects our use of a one-dimensional δ function to describe a three-dimensional condition and ensures that G has units of inverse volume. Scaling the

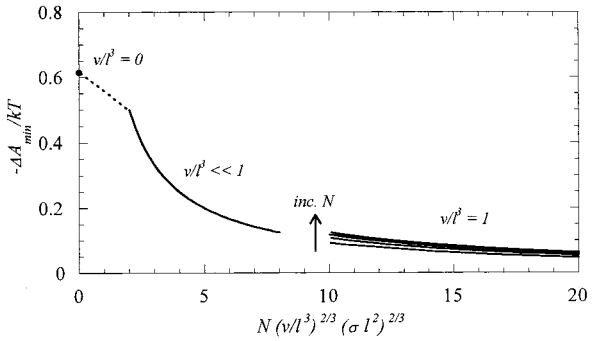

Figure 5. Attractive minima for telechelic polymers between flat plates, comparing our result for ideal chains ($v/l^3 = 0$) to the solutions for marginal (Milner and Witten)[16] and good (Björling[18] and Björling and Stilbs)[19] solvents. The ranges indicated on the *x*-axis are approximate.

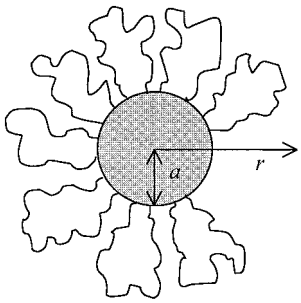

Figure 6. Telechelic chains attached to a sphere.

variables as $\bar{r} = r/N^{1/2}l$, $\bar{s} = s/N$, and $\bar{G} = 4\pi a^2 N^{1/2} l G$ yields two new dimensionless groups, $\bar{a} = a/N^{1/2}l$ and $\bar{r}_o = \bar{a} + {}^1/_2 N^{1/2}$, or $\bar{a}$ and N, on which $\bar{G}(\bar{r}, \bar{r}_o, \bar{s})$ depends. The system can be solved with Laplace transforms to obtain

$$G(r, r_o, s) = \left(\frac{3}{2\pi s l^2}\right)^{1/2}\left(\frac{r_o}{4\pi r a^2}\right) \times \left[\exp\left(-\frac{3(r - r_o)^2}{2sl^2}\right) - \exp\left(-\frac{3(r + r_o - 2a)^2}{2sl^2}\right)\right] \quad (21)$$

which corresponds roughly to Gaussian coils anchored to a spherical surface.

To calculate the free energy per chain for chains with only one end affixed to the sphere, we sum up the configurations for the entire chain, $s = N$, allowing the end of the chain to sample all space

$$\frac{A}{kT} = -\ln\left[\int_a^\infty 4\pi r^2 G(r, r_o, N)\, dr\right] \quad (22)$$

which yields

$$\frac{A}{kT} = -\ln\left[\left(1 + \frac{l}{2a}\right)\left\{\frac{l}{2a} + \mathrm{erf}\left(\sqrt{\frac{3}{8N}}\right)\right\}\right] \approx \frac{1}{2}\ln\left[\frac{2\pi N}{3}\right] - \ln\left[1 + \sqrt{\frac{\pi}{6}}\frac{N^{1/2}l}{a}\right] + O\left(\frac{l}{a}\right) + O\left(\frac{1}{N}\right) \quad (23)$$

Thus, curvature decreases the free energy below the flat plate limit of Dolan and Edwards.[11]

To obtain the free energy for chains with both ends attached to the sphere, we again allow the end to occupy the volume between $r = a$ and $r = a + l$, which is approximately $G(r = r_o)$ multiplied by l:

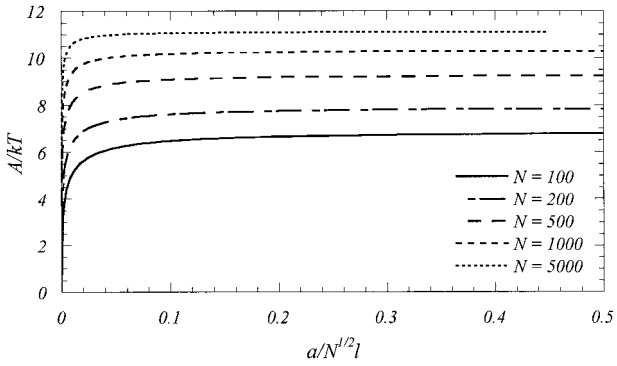

Figure 7. Free energy per chain for telechelic chains on an isolated particle as a function of chain length.

$$\frac{A}{kT} = -\ln\left[\int_a^{a+l} 4\pi r^2 G(r, r_o, N)\, dr\right] \approx -\ln[4\pi l r_o^2\, G(r_o, r_o, N)] \approx \frac{1}{2}\ln\left[\frac{2\pi N}{3}\right] + \ln\left[\frac{2N}{3}\right] + O\left(\frac{1}{N}\right) + O\left(\frac{l}{a}\right) \quad (24)$$

Just as in the case of flat plates, the additional constraint of having both ends on the surface increases the free energy by $\ln(2N/3)$. Thus, relative to loops on the flat plate, surface curvature only decreases the free energy by a small amount, $O(l/a)$. This effect can be seen in Figure 7, which shows the variation of the free energy with $a/N^{1/2}l$ and N and demonstrates that the free energy approaches the flat plate solution for telechelics at much lower values of $a/N^{1/2}l$ than for end-grafted polymers. Thus, the effect of surface curvature seems to be much less pronounced for telechelics than for end-grafted polymers.

The segment density for telechelic chains must be normalized to the total number of segments using the relation

$$n(r) = \frac{Np\int_0^N G(r, r_o, s)G(r, r_o, N - s)\, ds}{4\pi\int_a^\infty\int_0^N r^2 G(r, r_o, s)G(r, r_o, N - s)\, ds\, dr} \quad (25)$$

where p is the number of polymers per particle, so that the chain density on the surface is $n_p = p/4\pi a^2$. The segment density shown in Figure 8 resembles that in Figure 2 for flat plates, though increasing curvature allows the chains to relax toward the surface.

Numerical Results: Two Spheres

We next consider telechelic polymers between two interacting spheres. The formalism is the same but we must now solve the diffusion equation numerically in bispherical coordinates (μ, α, ϕ), also referred to as spherical bipolar coordinates (Figure 9). Readers wishing to know more about this coordinate system are referred to Morse and Feshbach.[23] The center-to-center distance between the two spheres is R, and the distance between the surfaces along the line of centers is $h = R - 2a$. The surfaces of the two spheres are $\mu = \mu_o$ and $\mu = -\mu_o$, with $\mu_o = \mathrm{arccosh}(R/2a)$. The coordinate α varies from 0 to π, with surfaces of constant α perpendicular to the spherical surfaces of constant μ. The surface $\alpha = \pi$ corresponds to the portion of the z-axis between the foci of the two spheres, while $\alpha = 0$

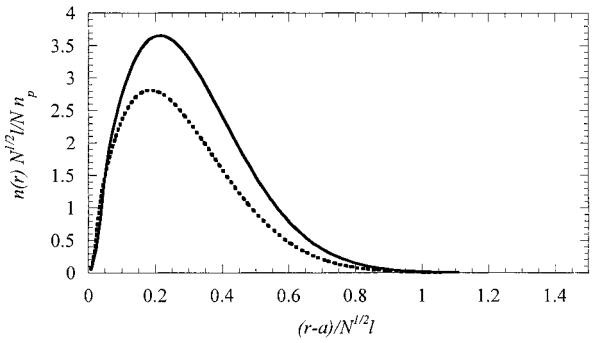

Figure 8. Segment density for telechelics adsorbed on an isolated particle. The dashed line is for $a/N^{1/2}l = 0.44$; the solid line is for $a/N^{1/2}l = 0.72$.

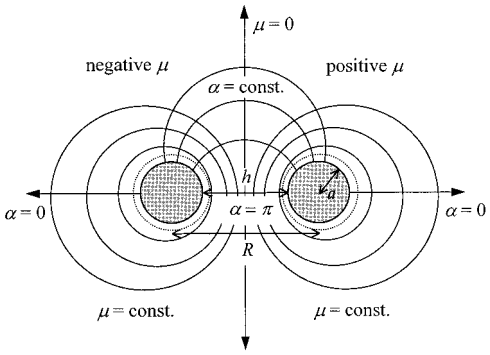

Figure 9. Bispherical coordinate system, showing two spheres of identical radius a at a center-to-center separation of R. The solid lines represent surfaces of constant μ and α. We consider chains to be attached to a surface that is $l/2$ off the spheres, represented by a dotted line. Note that μ is not constant over this surface.

corresponds to the z-axis outside the foci plus the sphere at infinity. The differential equation is

$$\frac{\partial G}{\partial s} = \frac{l^2}{6}\left(\frac{2}{R}\frac{\cosh\mu - \cos\alpha}{\tanh\mu_o}\right)^3 \times \left[\frac{\partial}{\partial\mu}\left(\frac{R}{2}\frac{\tanh\mu_o}{\cosh\mu - \cos\alpha}\frac{\partial G}{\partial\mu}\right) + \frac{1}{\sin\alpha}\frac{\partial}{\partial\alpha}\left(\frac{R}{2}\frac{\tanh\mu_o \sin\alpha}{\cosh\mu - \cos\alpha}\frac{\partial G}{\partial\alpha}\right)\right] \quad (26)$$

Note that the dimensionless coordinates μ and α appear as arguments of trigonometric functions in the above equation, while the physical dimensions enter through a scale factor, $R \tanh\mu_o = R[1 - (2a/R)^2]^{1/2}$. The scaling $\bar{s} = s/N$ and $\bar{G} = 4\pi a^2 N^{1/2} l G$ yields

$$\frac{\partial \bar{G}}{\partial \bar{s}} = \frac{2}{3}\frac{Nl^2}{(R+2a)(R-2a)}(\cosh\mu - \cos\alpha)^3 \times \left[\frac{\partial}{\partial\mu}\left(\frac{1}{\cosh\mu - \cos\alpha}\frac{\partial \bar{G}}{\partial\mu}\right) + \frac{1}{\sin\alpha}\frac{\partial}{\partial\alpha}\left(\frac{\sin\alpha}{\cosh\mu - \cos\alpha}\frac{\partial \bar{G}}{\partial\alpha}\right)\right] \quad (27)$$

and identifies the dimensionless groups $(R - 2a)/N^{1/2}l$ and $(R + 2a)/N^{1/2}l$ or, alternatively, $(R - 2a)/N^{1/2}l$ and $a/N^{1/2}l$.

We take the point of attachment to be $l/2$ off the surface of the right-hand sphere, and require that the chain not penetrate either sphere. This leads to the following initial and boundary conditions

$$\bar{G}(\mu, \alpha, 0) = \delta(\mu - \mu_o'(\alpha)) \quad (28a)$$

$$\bar{G}(\mu_o, \alpha, \bar{s}) = 0 \quad (28b)$$

$$\bar{G}(-\mu_o, \alpha, \bar{s}) = 0 \quad (28c)$$

where $\mu_o'(\alpha)$ represents the surface of a sphere of radius $a + l/2$, indicated by a dotted line in Figure 9. We also have a symmetry condition about the line of centers of the two spheres, which corresponds to $\alpha = 0$ and $\alpha = \pi$.

$$\left.\frac{\partial \bar{G}}{\partial\alpha}\right|_{\alpha=0} = 0 \quad (28d)$$

$$\left.\frac{\partial \bar{G}}{\partial\alpha}\right|_{\alpha=\pi} = 0 \quad (28e)$$

Finally we require that far away from the two spheres, $G = 0$, which is equivalent to

$$\bar{G}(0, 0, \bar{s}) = 0 \quad (28f)$$

While eq 28a is conceptually attractive as an initial condition, it is somewhat difficult to implement. In addition to numerical problems associated with the δ function, it is awkward to express the surface of two concentric spheres in bispherical coordinates. To circumvent this problem, we subtract the solution for the single sphere, eq 21, to eliminate the δ function in the initial condition and solve for the difference, $\Gamma = \bar{G}(\mu, \alpha, \bar{s}) - \bar{G}^{ss}(\bar{r}, \bar{s})$, which satisfies the same differential equation with modified initial and boundary conditions

$$\Gamma(\mu, \alpha, 0) = 0 \quad (29a)$$

$$\Gamma(\mu_o, \alpha, \bar{s}) = 0 \quad (29b)$$

$$\Gamma(-\mu_o, \alpha, \bar{s}) = -\bar{G}_{ss}(\bar{r}_1, \bar{s}) \quad (29c)$$

$$\left.\frac{\partial \Gamma}{\partial\alpha}\right|_{\alpha=0} = 0 \quad (29d)$$

$$\left.\frac{\partial \Gamma}{\partial\alpha}\right|_{\alpha=\pi} = 0 \quad (29e)$$

$$\Gamma(0, 0, \bar{s}) = 0 \quad (29f)$$

with

$$\bar{r}_1 = \frac{R}{2N^{1/2}l}\sqrt{\left(\frac{\tanh\mu_o \sinh\mu_o}{\cosh\mu_o - \cos\alpha} + 1\right)^2 + \left(\frac{\tanh\mu_o \sin\alpha}{\cosh\mu_o - \cos\alpha}\right)^2} \quad (30)$$

It is important to note that our initial condition now implicitly assumes that the chains start with equal probability anywhere on the sphere. At close separations, this might break down, since chain ends should be forced out of the gap between the two spheres.

We solve eqs 27 and 29 numerically using an explicit finite difference method spatially with step sizes of $\Delta\mu = 0.1$ and $\Delta\alpha = \pi/20$ and integrating forward along the chain using the Euler method with $\Delta\bar{s} = 0.015625$. The conditions for stability[24] are $\lambda_\mu \equiv \Delta\bar{s}/(\Delta\mu)^2 \leq 1/2$ and $\lambda_\alpha \equiv \Delta\bar{s}/(D\alpha)^2 \leq 1/2$. For the step sizes we have chosen, $\lambda_\mu = 0.156$ and $\lambda_\alpha = 0.158$, ensuring stability of our numerical solution. We will be most interested in the value of Γ for the entire chain, $\bar{s} = 1$, and by analogy

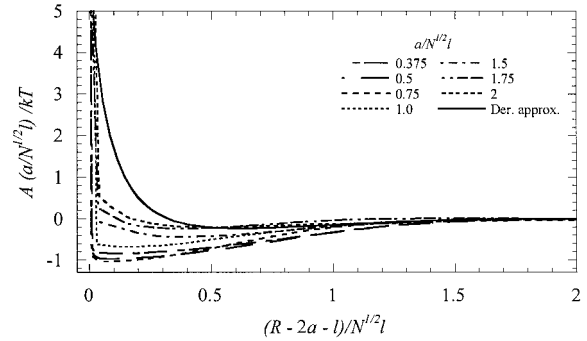

Figure 10. Free energy per chain scaled on $a/N^{1/2}l$ compared to the Derjaguin approximation.

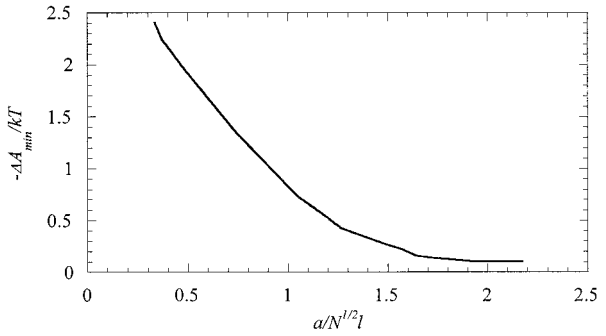

Figure 11. Depth of attractive minimum as a function of $a/N^{1/2}l$.

with the two-dimensional heat equation,[24] we expect the discretization error at this point to be $O(\Delta\bar{s} + (\Delta\mu)^2 + (\Delta\alpha)^2 \sim 0.05$. In practice, we find that when the step sizes are reduced, the numerical results for Γ converge to the same value; i.e., the solution method is convergent.

From the numerical solution for $\Gamma(\mu, \alpha, \bar{s})$, we compute the free energy at each separation by summing the number of configurations for loops and bridges and integrating over the surface of each sphere. The free energy is normalized on the free energy at infinite separation from the solution of the single sphere

$$\frac{\Delta A}{kT}(\bar{h}) = +\ln \bar{G}^{ss}(\mu_o', 1) - \ln\left(\frac{R^2}{8r_o^2} - \frac{1}{2}\right) - \ln\left[\int_0^{\pi} \frac{\sin\alpha}{(R/2r_o - \cos\alpha)^2}\{\bar{G}(\mu_o', \alpha, 1)_{\bar{h}} + \bar{G}(-\mu_o', \alpha, 1)_{\bar{h}}\}\, d\alpha\right] \quad (31)$$

where $-\mu_o'$ represents the surface $l/2$ off the left-hand sphere. As can be seen in Figure 9, this surface is not a surface of constant μ. Thus, it is sometimes necessary to interpolate between grid points to obtain the value of $\bar{G}$ this surface.

The results for selected values of $a/N^{1/2}l$ are shown in Figure 10. The attractive minimum is rather deep, varying monotonically from $-2.5\ kT$ to $-0.1\ kT$ per chain with increasing $a/N^{1/2}l$ (Figure 11). The repulsive part of the potential is very steep for small $a/N^{1/2}l$ and gradually becomes softer as surface curvature decreases. We can understand this trend by examining the probability density of bridging chain ends at the left sphere surface, $G(-\mu_o, \alpha, N)$, shown in Figure 12 for $a/N^{1/2}l = 0.375$. Recall that $\alpha = \pi$ corresponds to the line of centers between the two spheres, and $\alpha = 0$ is the symmetry axis outside the spheres. At large separations, the probability density is nearly uniform. As the spheres are brought closer together, the probability density at $\alpha = \pi$ increases as chains begin to bridge. However, the chains eventually are forced out of the gap, and the probability density begins to decrease at $\alpha = \pi$ and develops a maximum at $\alpha \cong \pi/2$ for $h/N^{1/2}l < 0.3$ that moves toward $\alpha = 0$ as $h/N^{1/2}l \rightarrow 0$. Thus, chains beginning in the gap preserve configurational degrees of freedom by moving the bulk of their segments out of the gap.

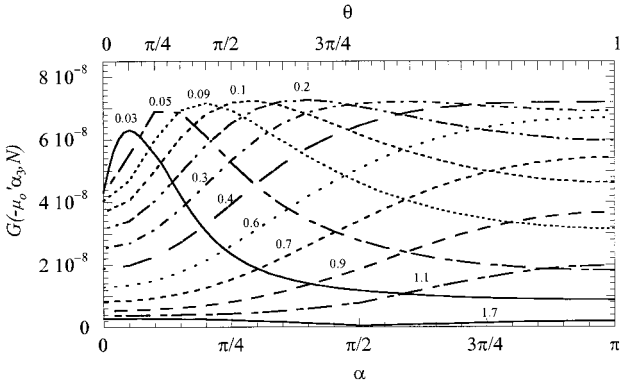

Figure 12. Probability density on the left sphere surface for $a/N^{1/2}l = 0.375$. The lines represent different normalized separations, $(R - 2a)/N^{1/2}l$. The lower axis is the bispherical coordinate α, and the upper axis is the spherical polar coordinate θ about the sphere, defined such that $\theta = 0$ corresponds to the surface furthest from the right sphere.

Because G must be integrated over the surface of the sphere to obtain significant physical quantities, it is somewhat misleading to compare the relative values of G at different separations to extract quantitative information about the free energy or segment density. We can, however, qualitatively explain the trends in the free energy that we observe. The attraction is due to bridging chains, the majority of which are in the gap between the two spheres at large separations. Although chains are excluded from the gap at closer separations, they will wrap around the far side of the sphere in order to bridge, leading to a strong attraction at all separations greater than l. At a separation of l, we obtain a hard-sphere repulsion, because of the boundary condition that starts the chain $l/2$ off the surface. For large $a/N^{1/2}l$, chains find it more difficult to move out of the gap, so both looped and bridging chains that remain in the gap and are compressed lead to a softer and longer range repulsion.

Our results are compared to the Derjaguin approximation based on the flat plate solution in Figure 10. For two spheres of radius a, the Derjaguin approximation is

$$\frac{\Phi_{sphere}}{kT} = \pi a \int_{r-2a}^{\infty} \frac{\Phi_{plate}}{kT}\, dx \quad (32)$$

where Φ_{plate} is the potential per unit area between flat plates. Relating the potentials for a sphere and flat plate to the free energy

$$\Phi_{sphere} = 2p\Delta A_{sphere} \quad (33a)$$

$$\Phi_{plate} = 2n_p\Delta A_{plate} = \frac{p}{2\pi a^2}\Delta A_{plate} \quad (33b)$$

yields the following approximation for the free energy:

$$\frac{\Delta A_{\text{sphere}}}{kT} = \frac{N^{1/2}l}{4a}\int_{\frac{r-2a}{N^{1/2}l}}^{\infty} \frac{\Delta A_{\text{plate}}}{kT}\, d\bar{x} \qquad (34)$$

This suggests scaling the free energy as

$$\bar{A} = \frac{\Delta A_{\text{sphere}}}{kT}\left(\frac{a}{N^{1/2}l}\right) \qquad (35)$$

As shown in Figure 10, this scaling appears to collapse the two-sphere solution for $0.375 \le a/N^{1/2}l \le 0.75$. The slight differences between the curves for $0.375 \le a/N^{1/2}l \le 0.75$ and the apparent nonmonotonic dependence of $A(a/N^{1/2}l)/kT$ on $a/N^{1/2}l$ in this range may be due in part to numerical errors associated with the finite difference method. For $a/N^{1/2}l \le 1$, the solution gradually moves forward to the Derjaguin approximation. In all cases, the Derjaguin approximation yields a stronger repulsion than the bispherical solution. This is consistent with the results of Wijmans et al.[15] and is most likely due to migration of polymers out of the gap in the case of two spheres.

Conclusions

We have used a diffusion-equation approach to model the segment density and free energy between surfaces covered with ideal end-capped associative polymer chains. The fraction of bridging chains increases as separation decreases, reaching a value of $^1/_3$ at close separations. We find an attractive minimum in the free energy in all cases. For flat plates, the attraction of 0.6 kT per chain occurs at a separation of roughly one end-to-end distance and is stronger than for marginal and good solvents, where typical values for the molecular weight and graft density yield attractions in the range $0.05-0.2kT$ per chain.[19] Our results and those of Björling and Stilbs[19] can be expressed in terms of the scaling proposed by Milner and Witten:[16] $\Delta A_{\text{min}}/kT \sim (R_0/L)^2$. Our result should represent an upper limit on the strength of attraction for associative systems.

Numerical results for chains between two spheres also indicate an $O(kT)$ attraction, occurring at a separation less than $N^{1/2}l$. The repulsion in this case is weaker than that given by the Derjaguin approximation. These effects are due to chains migrating out the gap between the two spheres.

Although we have only considered ideal chains, we expect chains in a good solvent should display qualitatively similar behavior. Chains attached to curved surfaces should have a lower free energy relative to chains attached to flat plates, although the effect may not be as important for telechelic chains as for end-grafted chains. Similar to what we observe for flat plates, we expect excluded volume effects to impart a stronger repulsion between the surfaces and perhaps a weaker attraction, in accord with the results of Santore et al.[17] and Björling and Stilbs.[19]

The force between flat plates with associative polymers can be measured directly using the surface forces apparatus. Given the correct experimental conditions, it should be possible to verify our results for flat plates. Dai and Toprakcioglu[25] and Dai et al.[26] report force curves for several triblock chains adsorbed to mica surfaces and find an attraction due to the bridging chains. However, the end blocks are not strongly absorbed, which results in a distribution of loops, bridges, and tails[25,26] that we have not considered in our theory. This problem may be overcome by using triblocks with longer or more strongly absorbed end blocks. Our results on spherical surfaces can be verified experimentally using osmotic pressure measurements or small-angle neutron scattering to estimate particle interaction potentials for colloids covered with associative polymers.

Our numerical results indicate that for $a/N^{1/2}l = O(1)$, the attractive interaction produced by telechelic polymers is fairly strong. For colloids in solution with associative polymers, this interaction can be several kT, large enough to cause flocculation. Similar results are expected for polymeric micelles of telechelics, which may lead to a phase separation, as predicted for micelles with high aggregation numbers by Semenov et al.[20] However, for chains in a good solvent, the attraction may be weaker and the tendency to phase separate may be suppressed.

Acknowledgment. This research was partially supported by fellowships from the Department of Defense and the American Association of University Women for S.R.B. and by the National Science Foundation through the Princeton Couter for Complex Materials (MRSEC DMR-9809488).

References and Notes

(1) Alexander, S. *J. Phys.* **1977**, *38*, 983−987.
(2) Milner, S. T.; Witten, T. A.; Cates, M. E. *Macromolecules* **1988**, *21*, 2610−2619.
(3) Wijmans, C. M.; Scheutjens, J. M. H. M.; Zhulina, E. B. *Macromolecules* **1992**, *25*, 2657−2665.
(4) Ruckenstein, E.; Buqiang, L. *J. Chem. Phys.* **1997**, *107*, 932−942.
(5) Carignano, M. A.; Szleifer, I. *Macromolecules* **1995**, *28*, 3197−3204.
(6) Carignano, M. A.; Szleifer, I. *Adv. Chem. Phys.* **1996**, *94*, 165−260.
(7) Zhulina, E. B.; Vilgis, T. A. *Macromolecules* **1995**, *28*, 1008−1015.
(8) Derjaguin, B. V. *Kolloid Z.* **1934**, *69*, 155−164.
(9) Daoud, M.; Cotton, J. P. *J. Phys.* **1982**, *43*, 531−538.
(10) Dan, N.; Tirrell, M. *Macromolecules* **1992**, *25*, 2890−2895.
(11) Dolan, A. K.; Edwards, S. F. *Proc. R. Soc. London* A **1974**, *337*, 509−516.
(12) Fleer, G. J.; Cohen Stuart, M. A.; Scheutjens, J. M. H. M.; Cosgrove, T.; Vincent, B. *Polymers at Interfaces*; Chapman and Hall: New York, 1993.
(13) Li, H.; Witten, T. A. *Macromolecules* **1994**, *27*, 449−457.
(14) Wijmans, C. M.; Zhulina, E. B. *Macromolecules* **1993**, *26*, 7214−7224.
(15) Wijmans, C. M.; Leermakers, F. A. M.; Fleer, G. J. *Langmuir* **1994**, *10*, 4514−4516.
(16) Milner, S. T.; Witten, T. A. *Macromolecules* **1992**, *25*, 5495−5503.
(17) Santore, M. M.; Russel, W. B.; Prud'homme, R. K. *Macromolecules* **1990**, *23*, 3821- 3822.
(18) Björling, M. *Macromolecules* **1998**, *31*, 9026−9032.
(19) Björling, M.; Stilbs, P. *Macromolecules* **1998**, *31*, 9033−9043.
(20) Semenov, A. N.; Joanny, J.-F.; Khokhlov, A. R. *Macromolecules* **1995**, *28*, 1066−1075.
(21) Johner, A.; Joanny, J.-F. *J. Chem. Phys.* **1992**, *96*, 6257−6273.
(22) Russel, W. B.; Saville, D. A.; Schowalter, W. R. *Colloidal Dispersions*; Cambridge University Press: New York, 1995.
(23) Morse, P. M.; Feshbach, H. *Methods of Theoretical Physics. Part II*. McGraw-Hill: New York, 1953.
(24) Isaacson, E.; Keller, H. B. *Analysis of Numerical Methods*; Dover Publications: New York, 1994.
(25) Dai, L.; Toprakcioglu, C. *Macromolecules* **1992**, *25*, 6000−6006.
(26) Dai, L.; Toprakcioglu, C.; Hadziioannou, G. *Macromolecules* **1995**, *28*, 5512−5517.

MA0000677